CO 2 Hydrogenation to Methanol Over Cu/ZnO/Al 2 O 3 Catalyst: Kinetic Modeling Based on Either Single-or Dual-Active Site Mechanism

Article *in* Catalysis Letters · January 2022

DOI: 10.1007/s10562-021-03913-0

CITATION
1

READS
135

8 authors, including:

Liuqingqing Yang
Shanghai Jiao Tong University
9 PUBLICATIONS **160** CITATIONS
SEE PROFILE

Ziyi Chi
Shanghai Jiao Tong University
4 PUBLICATIONS **20** CITATIONS
SEE PROFILE

Xue-Gang Li
Shanghai Jiao Tong University
20 PUBLICATIONS **108** CITATIONS
SEE PROFILE

Yulian He
Shanghai Jiao Tong University
27 PUBLICATIONS **262** CITATIONS
SEE PROFILE

Catalysis Letters
https://doi.org/10.1007/s10562-021-03913-0

CO_2 Hydrogenation to Methanol Over $Cu/ZnO/Al_2O_3$ Catalyst: Kinetic Modeling Based on Either Single- or Dual-Active Site Mechanism

Hou-Xing Li[1] · Liu-Qing-Qing Yang[2,3] · Zi-Yi Chi[1] · Yu-Ling Zhang[1] · Xue-Gang Li[1] · Yu-Lian He[2] · Tomas R. Reina[3] · Wen-De Xiao[1]

Received: 25 October 2021 / Accepted: 28 December 2021

Abstract

CO_2 hydrogenation to CH_3OH via heterogeneous catalysis is one of the most promising and available approaches for mitigation of anthropogenic CO_2 issues. In this work, thermodynamic equilibria of CO_2 to methanol were compared with experimental results at given conditions using a commercial $Cu/ZnO/Al_2O_3$ catalyst for CO hydrogenation to methanol. It was found that, the high pressure, low temperature, and high H_2/CO_2 ratio are favorable to methanol synthesis from CO_2. Furthermore, the kinetic data were measured with an isothermal integral reactor under temperature between 160 and 240 °C, lower than that for CO hydrogenation to methanol reaction. Based on the single-active site and dual-active site LH mechanisms, both kinetic models can achieve full illustration of the influence of the operating conditions and the mechanisms. According to comparative analysis of the error variances of model correlations and the adsorbate coverages on the active sites, the dual-site mechanism identified to be superior to the single-site one for methanol synthesis from CO_2 feedstock. Overall, this paper provides fundamental understanding of the thermodynamic and kinetic aspects of a central route for CO_2 Valorisation.

Hou-Xing Li and Liu-Qing-Qing Yang have equally contributed to this work.

✉ Wen-De Xiao
wdxiao@sjtu.edu.cn

[1] School of Chemistry and Chemical Engineering, Shanghai Jiao Tong University, 800 Dong-Chuan Road, Shanghai, People's Republic of China

[2] Present Address: UM-SJTU Joint Institute, Shanghai Jiao Tong University, 800 Dong-Chuan Road, Shanghai 200240, China

[3] Department of Chemical and Process Engineering, University of Surrey, Guildford, UK

Published online: 08 January 2022

Graphical Abstract

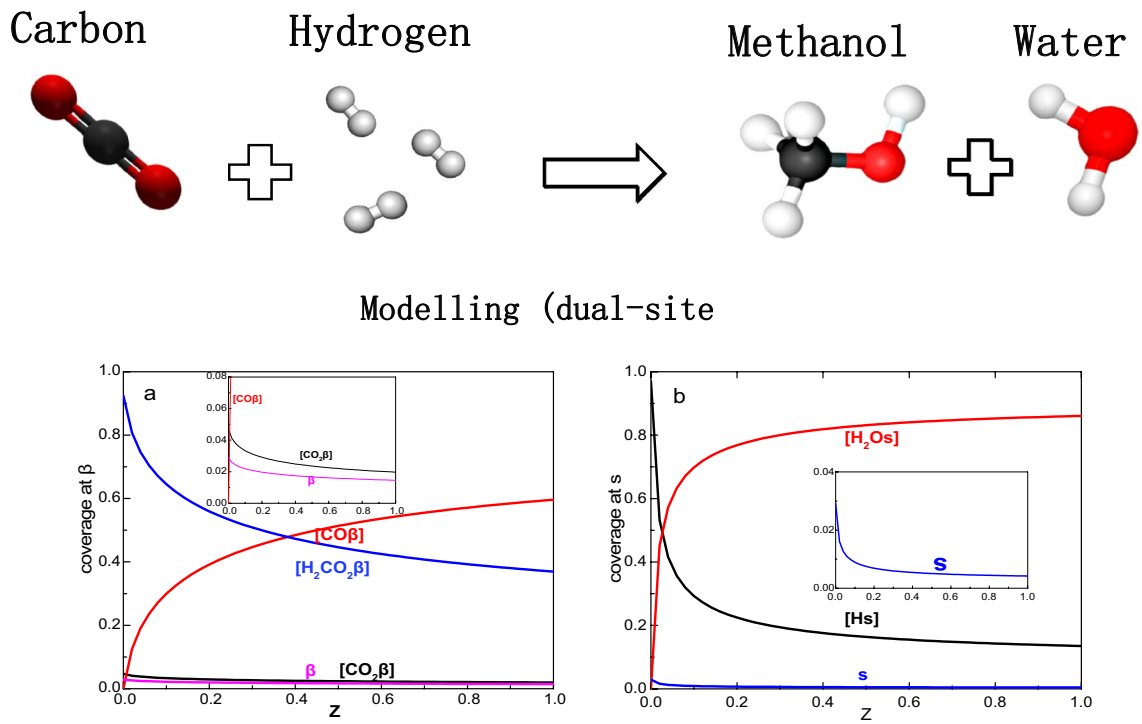

Keywords Carbon dioxide · Methanol · Reaction kinetics · Thermodynamic study · Copper-Zinc-Alumina

List of Symbols

A(i)	The pre-exponent constant
B(i)	Activation energy or heat of adsorption
H_2/CO_2	The ratio of H_2 to CO_2
Ki	Kinetic constant
P	Pressure, bar
S	Selectivity
T	Temperature, °C
X	Conversion Rate
$X_{CO_2}^{eq}$	Thermodynamic equilibrium conversion of CO_2
F	Ratio of regression mean square sum to model residual mean square sum
X_{CO_2}	Conversion of CO_2
S_{CO}	Selectivity of CO
S_{CH_3OH}	Selectivity of CH_3OH
W_{cat}	Loading quality of catalyst of Reactor inlet, g
r_m	The rate of reaction m, m = 1,2,mmol·g^{-1}·min^{-1}
$v_{m,i}$	The measurement coefficient of component i in reaction m

1 Introduction

CO_2 is a well-accepted greenhouse gas mostly produced from fossil fuel combustion. The steady increase of the atmospheric CO_2 level since the industry revolution has been considered as the main reason for the observed global warming and climate change [1–4]. Therefore, there is an urgent need to tackle excess CO_2 emission in the atmosphere. In this context, carbon capture and utilisation (CCU) has been initiated, aiming at generating value-added products from CO_2 waste, and become one of the most active research frontiers in energy and chemical engineering areas [5–8].

Among the developed CCU technologies, synthesis of methanol from CO_2 via heterogeneously catalytic hydrogenation is nearest to the practical application target and thus is quite attractive to the academia and industrial sectors as well. Indeed, Methanol is a viable energy carrier for vehicles and boilers and a key precursor for many high-value commodity chemicals, such as olefins by MTO technologies, formaldehyde for adhesives and resins [9–11]. Although the global methanol market is persistently growing, methanol is

mainly synthesised from syngas via coal/natural gas gasification. Therefore, the catalytic methanol synthesis from CO_2 has great potential for large-scale application on the basis of both economic and environmental concerns [12–14]. Furthermore, this route requires hydrogen supply which can be produced from the electrolysis of water using renewable energy sources [15–18]. In this sense, it represents an encouraging pathway for clean hydrogen production that supports the CO_2 utilisation leading to a green hydrogen-CO_2 nexus which is worth intensively exploring [19, 20].

It can be convinced that the most effective catalysts for the methanol synthesis are Cu-based, specifically, Cu/ZnO/Al_2O_3, due to its low cost, high activity and selectivity to methanol in the conventional methanol industry, and the well-established experiences can be easily adapted for the development of CO_2 hydrogenation to methanol. Moreover, as a general research rule, the kinetic study is deemed to be the essential step for reactor design and process development. Though many kinds of kinetic models have been proposed to describe the methanol synthesis where CO is assumed to be the feedstock in traditional methanol manufacturing routes [21–23]. Interestingly, in practice, CO_2 is required to add into the feed mixture to enhance the reaction rate of methanol synthesis, and many previous studies assumed that the carbon resource of methanol is directly from CO_2 according to the reaction of CO_2 hydrogenation co-producing H_2O, which then is immediately consumed by the followed water–gas shift reaction (WGS) with CO regenerating CO_2 and H_2 to make the overall reaction behaves as the CO hydrogenation [24–27]. At present, the kinetics of the reactions have been mostly developed on the basis of a power-law model or a Langmuir–Hinshelwood (L–H) model for methanol synthesis using only CO_2 [28]. For instance, Ledakowicz et al. examined several Cu/ZnO/Al_2O_3 catalysts for CO_2 methanol synthesis using a purely empirical power-law rate equation, but found that the experimental data presented 25% relative error to fit the model parameters [29]. Besides, Kobl et al. investigated the power-law models for methanol synthesis from CO_2/H_2 on Cu/ZnO/Al_2O_3 and Cu/ZnO/ZrO_2 catalysts, respectively, and found that the catalyst tests fits the model when the obtained conversions were less than 15% [30]. In this sense, the drawback of applying a power-law to this process is significant where the range of partial pressures, conversions and temperatures has to be defined. By contrast, the L–H model is a relatively complex kinetic model which is still under debate in CO_2 hydrogenation to methanol. For instance, Rasmussen et al. studied the synthesis of methanol from a fixed gas of H_2:CO_2 = 1:1 over a Cu(100) single crystal to give a modified L–H kinetic model based on the hydrogenation of dioxomethylene as the rate limiting step, with the presented kinetic model applied for semi-quantitative predictions of the reaction rates over a commercial catalyst working under industrial conditions for this process [31]. Portha et al. also attempted to determine a L–H kinetic model that enables sizing an industrial and delocalised reactor with reliability for pure CO_2 hydrogenation to methanol. Although no CO was included in the feed gas, for this work, all three reversible reactions (Eq. (1), Eq. (2), and Eq. (3)) were considered [32].

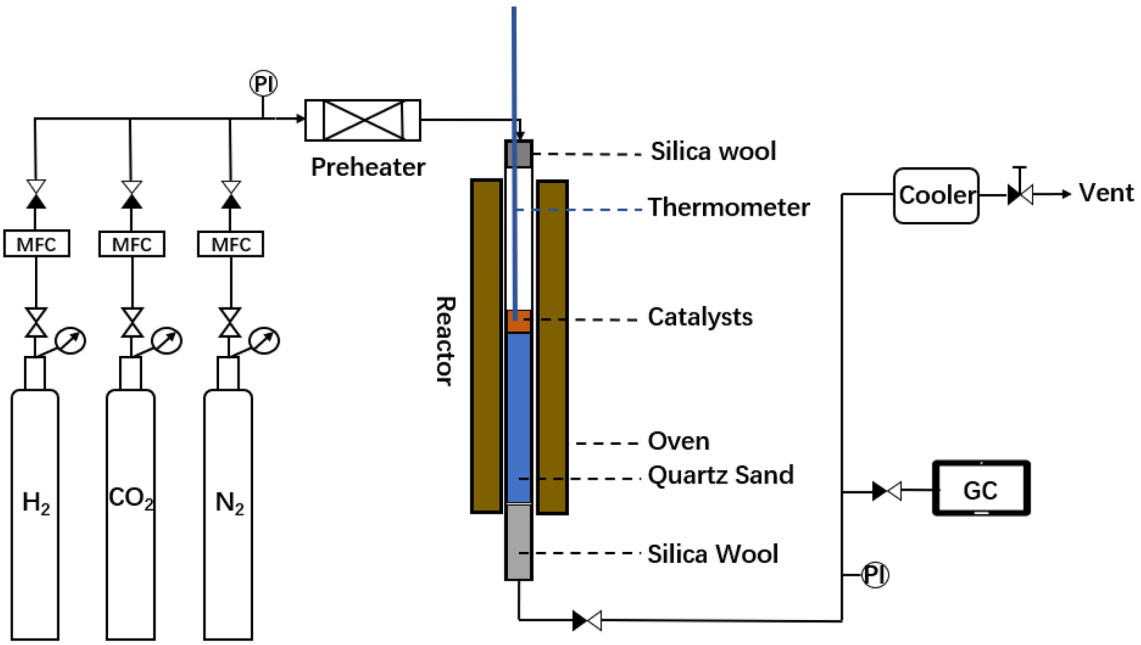

Fig. 1 Schematic diagram of CO_2 hydrogenation to methanol reaction process

$$CO + 2H_2 \leftrightarrow CH_3OH;\ \Delta H^o_{295K} = -90.5kJ/mol \quad (1)$$

$$CO_2 + H_2 \leftrightarrow CO + H_2O;\ \Delta H^o_{295K} = 41.1kJ/mol \quad (2)$$

$$CO_2 + 3H_2 \leftrightarrow CH_3OH + H_2O;\ \Delta H^o_{295K} = -49.4kJ/mol \quad (3)$$

To avoid this uncertainty, another kinetic model was established by Vanden Bussche and Froment when they studied a commercial $CuO/ZnO/Al_2O_3$ catalyst for methanol synthesis [25]. In this kinetic model, only the RWGS reaction (Eq. (2)) and the carbon dioxide hydrogenation (Eq. (3)) were considered, as it was assumed that CO_2 obtained from Eq. (2) was the main carbon source in further methanol synthesis through HCOO and a dissociative adsorption of H_2 and CO_2 was the rate-limiting steps [25]. As a matter of fact, Chinchen et al. assumed that CO_2 was the main source of methanol in 1986 [33]. Besides, through infrared spectroscopy, Clarke et al. found that the hydrogenation rate of CO_2 to methanol was much higher than the hydrogenation rate of CO to methanol, and the water gas conversion reaction between CO and water eliminated the H_2O molecules generated by the hydrogenation of CO_2, thus promoting the hydrogenation of CO_2 to methanol again [34].

Under this scenario of intense debate around kinetics of direct methanol production from CO_2, we present and compare two kinetic models considering the thermodynamic equilibrium and based on the study of Vanden Bussche and Froment and Graaf et al. [24, 25], respectively, over a commercial $Cu/ZnO/Al_2O_3$ catalyst (XNC-98, the low-pressure type, by Southwest Institute of Chemical Engineering, China). This study will account for the RWGS reaction as dominant side reaction, and the CO_2 hydrogenation to methanol as central process, in order to shed lights on the fundamental kinetic aspects of this crucial route for CO_2 transformation.

2 Experimental

2.1 Thermodynamic Prediction

Balanced conversion and product selectivity were estimated using Aspen Plus V.8.4 software. Phase equilibrium and chemical equilibrium are measured by RGibbs module method, and the Gibbs free energy is minimized to obtain the equilibrium state of a system with a group of chemical components at any given temperature and pressure. The usual RGibbs analysis requires only pressure and temperature and specified quantity of substance conditions, without the need for specific reaction equations and kinetics. In this study, the Peng-Robinson method, the interaction parameters within ASPEN and the binary interaction parameters were adopted. The selected reactants are CO_2, H_2 and products are CO, CH_3OH and H_2O.The yield of the higher alcohols and CH_4 under the reaction conditions were so small as to be negligible that it was not analysed. After the results of the first reaction run at 200 °C, pressure 2 Mpa and the H/C ratio of 3, the sensitivity analysis module was defined using different temperatures (140–280 °C), different pressures (0.5–3.0 Mpa) and different H/C ratio (2–10) for calculation.

2.2 Experimental Measurement

Catalytic reactions were performed on a fixed-bed reactor shown in Fig. 1, which was composed of a titanium alloys tube with an internal diameter of 8 mm and a total length of 760 mm. The catalyst bed consisted of a mixture of the 40–60 mesh of catalyst powder and quartz sand with a volume ratio of 2/3 to obtain an isothermal bed. Then a thermocouple was inserted to control the temperature of the reaction bed, and the reaction pressure was controlled by a back-pressure valve at the end of the reactor. In order to realize an isothermal temperature of the fixed bed reactor, a tubular furnace made by three-stage ovens was applied. Temperatures were well regulated via three stages' controllers at the top, at the middle, and at the bottom. The catalyst was loaded in the reactor and reduced at 200 °C for 12 h by mixture of ~ 5%H_2/N_2 (mole) with total flow rate of 150 mL/min. After the reduction, the catalyst was cooled down to 160 °C with varied feed gas compositions before increasing reaction pressure. The reaction temperature and pressure were kept at 160/180/200/220/250 °C and 1/1.5/2/2.5 MPa, respectively.

All the products were kept at 140 °C and analysed by online gas chromatography equipped with a thermal conductivity detector (TCD) and a flame ionization detector (FID). The Gas Chromatograph was equipped with PH-PONA chromatography column to analyze CH_3OH by FID detector, and carbon molecular sieves packed column to analyze N_2, CO, CH_4, CO_2 by TCD detector. The activity data used for discussion was collected 10 h after the catalyst was on stream. The conversion of CO_2, the selectivity of CO and CH_3OH was calculated by the following equations:

$$X_{CO_2} = \frac{F_{CO_2,in} - F_{CO_2}}{F_{CO_2,in}} \quad (4)$$

$$S_{CH_3OH} = 1 - S_{CO} \quad (5)$$

$$S_{CO} = \frac{F_{CO}}{F_{CO_2,in} - F_{CO_2}} \quad (6)$$

Table 1 Elementary steps in single-site kinetic mechanism (adapted based on Vanden Bussche and Froment [25], s represents the single surface-active site)

Step	Elementary steps
s1	$H_2(g)+2\,s \rightleftharpoons 2H.s$
s2	$CO_2(g)+s \rightleftharpoons CO_2.s$
s3	$CO_2.s+s \rightleftharpoons O.s+CO.s$
s4	$O.s+H.s \rightleftharpoons OH.s+s$
s5	$OH.s+H.s \rightleftharpoons H_2O.s+s$
s6	$CO_2.s+OH.s \rightleftharpoons HCO_3.2\,s$
s7	$HCO_3.2\,s+s \rightleftharpoons HCO_2.2\,s+O.s$
s8	$HCO_2.2\,s+H.s \rightleftharpoons H_2CO_2.2\,s+s$
s9	$H_2CO_2.2\,s \rightleftharpoons H_2CO.s+O.s$
s10	$H_2CO.s+H.s \rightleftharpoons H_3CO.s+s$
s11	$H_3CO.s+H.s \rightleftharpoons CH_3OH(g)+2\,s$
s12	$CO.s \rightleftharpoons CO(g)+s$
s13	$H_2O.s \rightleftharpoons H_2O(g)+s$

Table 2 Elementary steps in dual-site mechanism (s and β represent the dual surface-active sites, respectively. The elementary steps are based on the work of Graaf et al. [24])

Step	Elementary steps
d1	$H_2(g)+2\,s \rightleftharpoons 2H.s$
d2	$CO_2(g)+\beta \rightleftharpoons +CO_2.\beta$
d3	$CO_2.\beta+H.s \rightleftharpoons HCO_2.\beta+s$
d4	$HCO_2.\beta+H.s \rightleftharpoons H_2CO_2.\beta+s$
d5	$H_2CO_2.\,\beta+H.s \rightleftharpoons HCO.\,\beta+H_2O.s$
d6	$H_2CO_2.\,\beta+s \rightleftharpoons CO.\,\beta+H_2O.s$
d7	$HCO.\,\beta+H.s \rightleftharpoons H_2CO.\beta+s$
d8	$H_2CO.\,\beta+H.s \rightleftharpoons H_3CO.\beta+s$
d9	$H_3CO.\,\beta+H.s \rightleftharpoons H_4CO.\beta+s$
d10	$H_4CO.\beta \rightleftharpoons CH_3OH(g)+\beta$
d11	$CO.\,\beta \rightleftharpoons CO(g)+\beta$
d12	$H_2O.s \rightleftharpoons H_2O(g)+s$

where, $F_{CO_2,in}$ is the molar flow rate of CO_2 flowing into the reactor; F_{CO} is the molar flow rate of CO flowing out the reactor; and F_{CO_2} is the molar flow rate of CO_2 flowing out the reactor. For each data point, the result was obtained after the reaction reached steady-state. The error in CO_2 conversion and CO/CH_3OH selectivity for all the experiments is within ± 0.5% due the facility setup.

For the kinetic study, the effects of internal and external diffusion must be eliminated before tests. Internal diffusion can be eliminated by reducing the particle size of the catalyst. Catalysts with 20–40 mesh, 40–60 mesh, 60–80 mesh and 80–100 mesh were tested. When the number of catalyst mesh was greater than 40 mesh, the CO_2 conversion rate was basically unchanged. Therefore, the effect of internal diffusion has been eliminated by using 40–60 mesh catalyst. External diffusion can be eliminated by increasing the gas velocity of the reaction gas. The space velocity was kept unchanged at 12,000 $mL{\cdot}h^{-1}{\cdot}g^{-1}$, and the space velocity was changed by changing the flow rate and catalyst mass. When the flow rate was greater than 100 $mL{\cdot}min^{-1}$, the CO_2 conversion rate was basically unchanged. Therefore, the influence of external diffusion has been eliminated when the kinetic data retention flow is greater than 100 $ml{\cdot}min^{-1}$. In summary, kinetic experimental conditions are 40–60 mesh catalyst for 1 g, varied feed gas compositions were applied, total flow rate is greater than 100 $mL{\cdot}min^{-1}$, and reaction temperature 160–240 °C.

2.3 Mechanism and Kinetics

There are two reaction pathways for methanol from CO_2 hydrogenation proposed in the previous literatures. The first is the direct CO_2 hydrogenation to methanol through the formate intermediate, and the second involves the formation of CO from CO_2 through the RWGS reaction and then CO is hydrogenated to methanol. Several kinetic models have been developed for modeling methanol synthesis. Graaf et al. [24] proposed a dual site mechanism, one active site for CO and CO_2 adsorption and one for H_2 and H_2O adsorption. Vanden Bussche and Froment [25] proposed a single-site mechanism, including H_2 and H_2O, and the intermediate atomic O as well, but neglecting the adsorption of CO and CO_2. Ovesen et al. [26] proposed a dual-site mechanism, with one active site for CO adsorption and another one for CO_2 adsorption. Park et al. and Seidel et al. [27, 28] proposed three active sites for the adsorptions of CO, CO_2 and H_2/H_2O, respectively. In this work, the single-site and dual-site mechanisms will be focused on.

2.3.1 Single-Site Model

As given by Vanden Bussche and Froment [25], methanol was assumed to be generated only from CO_2 with the co-product water participating in the water–gas shift reaction, and the reaction kinetic model was constructed based on a single-site Langmuir–Hinshelwood mechanism, with the individual elementary steps shown in Table 1. Virtually, this mechanism can be regarded as the redox mechanism, where, CO_2 is an oxidant, and easily makes the active site, the metallic copper phase, be oxidized and produce CO to conduct the reverse water gas shift reaction with the followed reduction by the adsorbed hydrogen to release a molecule of water. For methanol, a carbonate intermediate appears primarily, by reaction of adsorbed CO_2 and the hydroxyl. The carbonate is quickly hydrogenated to formate, formaldehyde,

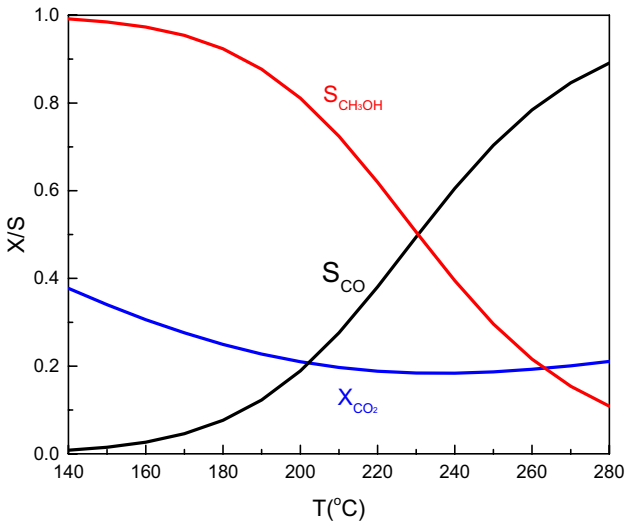

Fig. 2 Temperature influence on CO_2 conversion and product selectivity at thermodynamic equilibrium at 2.0 MPa and H_2:CO_2 = 3:1

methoxy species, and finally methanol. In this mechanism, the rate-determining step (RDS) is supposed to be hydrogenation of formate, which is well accepted to be the longest living intermediate in methanol synthesis on copper-based catalyst in the previous works [25].

With the assumption of the rate-determining step (RDS), step s3 for carbon monoxide and step s8 for methanol, the set of reaction rate equations are derived as follows based on a pseudo-steady-state hypothesis of the surface intermediates. (see nomenclature table for abbreviation) [25].

$$r_1 = \frac{k_1 \cdot P_{CO2} \cdot P_{H2} \cdot \left(1 - \frac{P_{CH3OH} \cdot P_{H2O}}{K_1 \cdot P_{H2}^3 \cdot P_{CO2}}\right)}{\left(1 + K_a \cdot \sqrt{P_{H2}} + K_b \cdot P_{H2O} + K_c \cdot \frac{P_{H2O}}{P_{H2}}\right)^3} \tag{7}$$

$$r_2 = \frac{k_2 \cdot P_{CO2} \cdot \left(1 - \frac{P_{CO} \cdot P_{H2O}}{K_2 \cdot P_{H2} \cdot P_{CO2}}\right)}{\left(1 + K_a \cdot \sqrt{P_{H2}} + K_b \cdot P_{H2O} + K_c \cdot \frac{P_{H2O}}{P_{H2}}\right)} \tag{8}$$

$$K_1 = \frac{3066}{T} - 10.592 \tag{9}$$

$$K_2 = \frac{-2073}{T} + 2.029 \tag{10}$$

$$k_i = A_i \exp\left(-\frac{B_i}{R}\left(\frac{1}{T} - \frac{1}{473.15}\right)\right),\ i = 1, 2 \tag{11}$$

$$K_i = A_i \exp\left(-\frac{B_i}{R}\left(\frac{1}{T} - \frac{1}{473.15}\right)\right),\ i = a, b, c \tag{12}$$

where, 200 °C < T < 300 °C; Kc is a combined adsorption constant including steps s1 and s10-s12, implying the adsorption of oxygen radical (given by the reaction of O.s + H_2(g) ⇌ H_2O(g) + s), and K_1 and K_2 are the thermodynamic equilibrium constants determined by Graaf et al. [35].

2.3.2 Dual-Site Model

A dual-site adsorption mechanism was proposed by Graaf et al. [24], giving that methanol could be generated from both CO and CO_2. In this work, the hydrogenation of CO_2 is assumed to be composed of Reaction (3) for methanol and water generation from CO_2 and H_2, and Reaction (2) for reverse water gas shift to generate CO and water, and to comply with the dual-site Langmuir–Hinshelwood mechanism, in which one site (β) was devoted to adsorb CO and CO_2, and the other site (s) to H_2 and H_2O [24]. In this sense, the following elementary steps are proposed according to the mentioned reaction mechanism above, see Table 2.

The total pathway consists of 12 elementary steps, with a common intermediate, formate, [H_2COO], for both methanol and CO formation. Key adsorbed intermediates are considered in the present work (via term $K_{a3}P_{CO_2}P_{H_2}$) in order to fully illustrate the dual-site mechanism. According to the previous researches on the water gas shift reaction by Yoshihara et al. [36], Ayastuy et al. [37], Mendes et al. [38], Madon et al.[39], and Kunkes et al. [40], [H_2COO] is apt to decompose into CO and H_2O on the surface active site, see step d6 in Table 2. For methanol formation, from hydrogenation of formate or formic acid, an intermediate, formyl, [HCO] appears with the release of a molecule of water on the surface site, which is sequentially hydrogenated to formaldehyde [H_2CO], methoxyl [H_3CO] and finally to

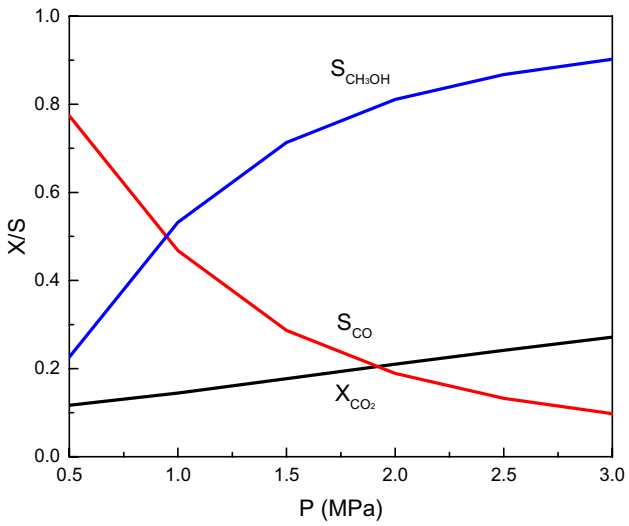

Fig. 3 Pressure influence on CO_2 conversion and product selectivity at thermodynamic equilibrium at 200 °C and H_2:CO_2 = 3:1

methanol. Based on the RDS theory, methanol is assumed to be determined by step d5 and CO by step d6, the set of reaction rate functions is obtained as follows (see nomenclature table for abbreviation).

$$r_1 = \frac{k_1\left(P_{H_2}^{1.5}P_{CO_2} - \frac{P_{MeOH}P_{H_2O}}{K_{eq1}P_{H_2}^{1.5}}\right)}{\left(1 + K_{a1}P_{CO_2} + K_{a2}P_{CO} + K_{a3}P_{CO_2}P_{H_2}\right)\left(1 + K_{b1}P_{H_2}^{0.5} + K_{b2}P_{H_2O}\right)} \quad (13)$$

$$r_2 = \frac{k_2\left(P_{H_2}P_{CO_2} - \frac{P_{CO}P_{H_2O}}{K_{eq2}}\right)}{\left(1 + K_{a1}P_{CO_2} + K_{a2}P_{CO} + K_{a3}P_{CO_2}P_{H_2}\right)\left(1 + K_{b1}P_{H_2}^{0.5} + K_{b2}P_{H_2O}\right)} \quad (14)$$

$$k_i = A_i \exp(-\frac{B_i}{R}\left(\frac{1}{T} - \frac{1}{473.15}\right)),\ i = 1, 2 \quad (15)$$

$$K_i = A_i \exp(-\frac{B_i}{R}\left(\frac{1}{T} - \frac{1}{473.15}\right)),\ i = a_1, a_2, b_1, b_2 \quad (16)$$

where, 200 °C < T < 300 °C, k_{a3}, is a combination of step d1-d4, meaning the adsorption of formate, and K_1 (Eq. (9)) and K_2 (Eq. (10)) are also the thermodynamic equilibrium constants determined by Graaf et al. [35].

3 Results and Discussion

3.1 Thermodynamic Simulations

In this work, the thermodynamic equilibrium of CO_2, H_2, CO, CH_3OH and H_2O under different conditions was simulated by RGibbs reactor in Aspen Plus V8.4, and the corresponding equilibrium composition was compared as follows.

First of all, the effect of reaction temperature on CO_2 conversion and selectivity is shown in Fig. 2. It can be seen that by rising the temperature from 140 to 280 °C, the selectivity of methanol decreases sharply, while the CO selectivity presents a significant increase. This trend reflects the thermodynamic nature of these two reactions. While the hydrogenation of CO_2 to produce methanol is an exothermic process, the RWGS reaction is an endothermic reaction favoured in the high temperature window. Therefore, the increasing of reaction temperature would inhibit the production of methanol, but promote CO formation. At the same time, CO_2 conversion initially shows a gradually decreasing with heating up, then recovering by the further temperature rise. Again, this represents the coupling of two reactions during the entire process, where the CO_2 hydrogenation to methanol dominates the process at a relatively low temperature, but the RWGS reaction becomes dominant when the reaction temperature increases to 230 °C and beyond.

Then the reaction temperature was fixed to 200 °C for the hereafter thermodynamic simulations and the effect of reaction pressure is presented in Fig. 3. It can be seen that CO_2 conversion shows a trend of mildly increasing with the pressure increasing in a manner of linearity. This can be explained by the Le Chatelier's principle: methanol synthesis is favoured by increasing total pressure. Besides, as the pressure increases, the selectivity of methanol gradually rise, while the selectivity of CO drops, and the methanol synthesis reaction becomes dominant when the reaction pressure increases to1.0Mpa and beyond.

Lastly, the impact of the feed composition is given in Fig. 4 under temperature of 200 °C, and pressure of 2.0Mpa.

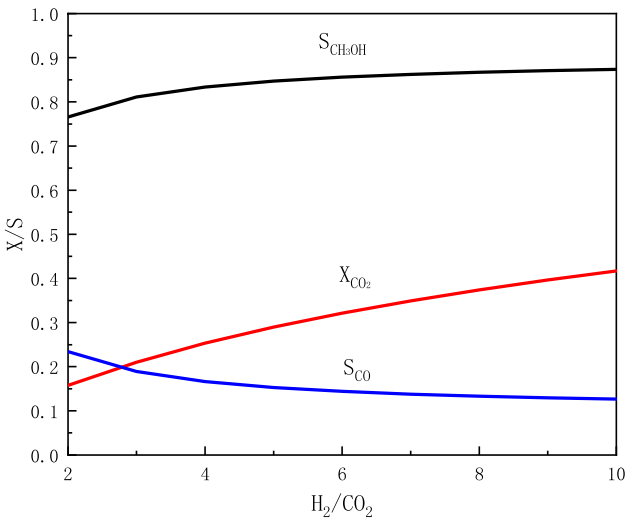

Fig. 4 Influence of H_2/CO_2 ratio on CO_2 conversion and product selectivity at thermodynamic equilibrium at 200 °C and 2.0 MPa

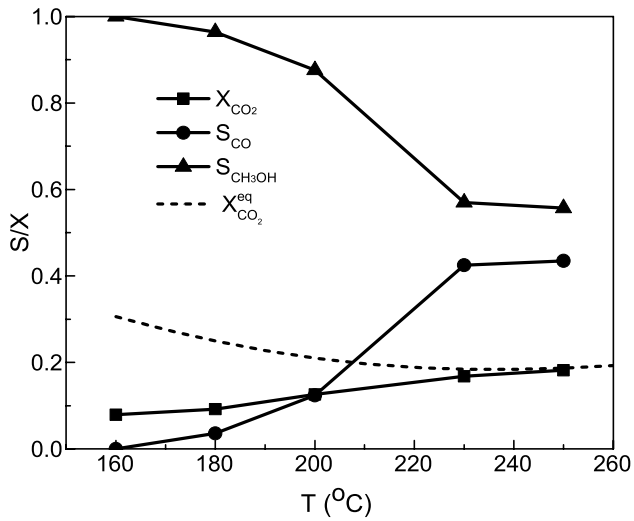

Fig. 5 Temperature influence on CO_2 conversion and product selectivity at 2 MPa, WHSV = 12,000 ml·g^{-1}·h^{-1} and H_2:CO_2 = 3:1

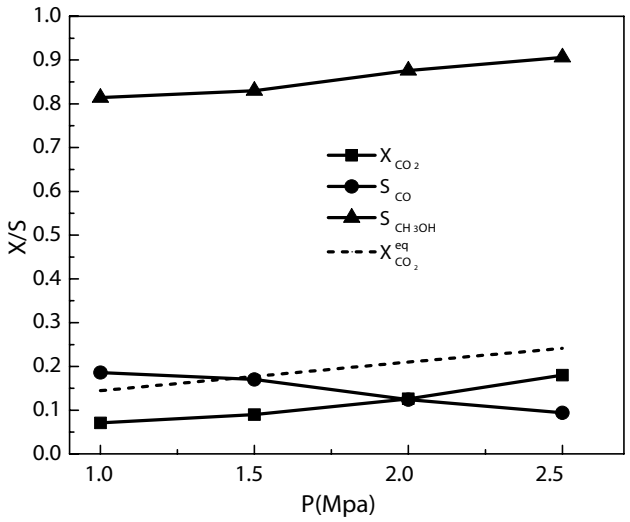

Fig. 6 Pressure influence on CO_2 conversion and product selectivity at 200 °C, WHSV = 12,000 ml·g^{-1}·h^{-1} and H_2:CO_2 = 3:1

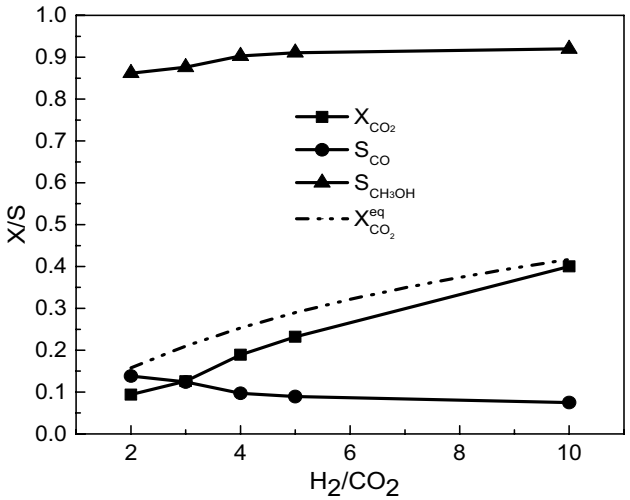

Fig. 7 Influence of H_2/CO_2 on CO_2 conversion and product selectivity of carbon dioxide hydrogenation at different H/C ratio (200 °C, WHSV = 12,000 ml·g^{-1}·h^{-1}, 2.0 MPa)

It can be seen that when the ratio of H_2/CO_2 increases, the selectivity of methanol gradually approaches 0.85 at 4.0 and beyond, and then comes to a plateau of about 0.90. By comparison, the CO selectivity decreases to 0.15 then becomes relatively stable. From the perspective of industrial application, an increasing concentration of hydrogen could facilitate the conversion of CO_2 in the reactor. However, an excessively high H_2/CO_2 ratio would significantly increase the energy consumption of the entire reaction system. Therefore, the thermodynamic simulation using different H_2/CO_2 ratios is essential to set a sensible H_2/CO_2 balance prior to conducting experiments. Nevertheless, considering that clean hydrogen could be generated via water electrolysis driven by renewable energy sources (i.e. wind), the overall process of methanol synthesis will be less cost and energy-intensive. While the consumption of the co-reactant, CO_2, is considered as a promising method for mitigation the CO_2 emission from the anthropogenic activities [5].

Take a summary from the thermodynamic study, one can notice that methanol synthesis from CO_2 hydrogenation is favoured by low reaction temperatures, high total pressure and high H_2/CO_2 ratio in the feed mixture. Besides, feasible operating conditions can be primarily defined in order to guide further catalytic tests.

3.2 Catalytic Activity and Selectivity

Following the discussion above, a series of catalytic tests at different operating conditions were carried out in a fixed-bed reactor (Fig. 1), using a commercial $Cu/ZnO/Al_2O_3$ catalyst for CO_2 hydrogenation to methanol.

First of all, the catalyst was tested within a temperature range of 160–250 °C. The reactants flow was held at a constant weight hourly space velocity (WHSV) of 12,000 ml·g^{-1}·h^{-1} with a H_2/CO_2 ratio of 3:1. From Fig. 5, it can be seen that as the thermodynamic equilibrium is far from being reached at the temperature lower than 220 °C, an increasing of reaction temperature from 160 °C has significant influence on both CO_2 conversion and product selectivity. At temperature higher than 230 °C, both reactions of methanol synthesis and reverse water gas shift to CO are closed to the equilibrium states. Moreover, it can be noticed that methanol synthesis is favoured when the temperature is less than 200 °C, while the production of CO emerges obviously when the temperature reaches to 200 °C and beyond. Interestingly, CO_2 conversion shows an opposite trend to the thermodynamic equilibrium curve, where it decreases with temperature, which reflects the impact of the catalysts on the reaction kinetics as we will discuss in the next section.

A pressure screening (1.0 to 2.5 MPa) was then conducted using the commercial catalysts at fixed temperature, space velocity (WHSV) and reactants ratio: 200 °C, 12,000 ml·g^{-1}·h^{-1} and H_2/CO_2 ratio of 3:1. Figure 6 shows the results of the pressure influence. Again, upon increasing of reaction pressure, CO_2 conversion and methanol selectivity gradually increase, while CO selectivity decreases. This is in a good agreement with the above-mentioned results by the thermodynamic simulation. At 200 °C, the favorable reaction is methanol synthesis, which reduces the gas volume with pressure rise. By contrast, the RWGS reaction is not affected by an increase of total pressure as predicted by thermodynamics since the reactant presents same number of moles at both sides of the equilibrium equation.

Lastly, the catalyst was tested to investigate the effect of H2/CO2 ratio at 200 °C, 2.0 MPa and the WHSV of

Table 3 Experimental results of kinetic measurements

T (°C)	P (atm)	$F_{i,in}$(mmol·min^{-1})[a]			$F_{i,out}$(mmol·min^{-1})[b]					
		N_2	CO_2	H_2	N_2	CO_2	H_2	CH_3OH	CO	H_2O
200	20	1.78	2.38	4.76	1.78	2.16	4.15	0.19	0.03	0.22
200	20	1.78	1.78	5.35	1.78	1.56	4.74	0.2	0.03	0.22
160	20	1.78	1.78	5.35	1.78	1.64	4.93	0.14	0	0.14
180	20	1.78	1.78	5.35	1.78	1.62	4.87	0.16	0.01	0.16
230	20	1.78	1.78	5.35	1.78	1.48	4.71	0.17	0.13	0.3
200	10	1.78	1.78	5.35	1.78	1.66	5.02	0.1	0.02	0.13
200	15	1.78	1.78	5.35	1.78	1.62	4.93	0.13	0.03	0.16
200	20	1.34	1.34	4.01	1.34	1.14	3.46	0.18	0.03	0.2
200	20	1.78	1.78	5.35	1.78	1.56	4.74	0.2	0.03	0.22
200	20	2.23	2.23	6.69	2.23	2.01	6.1	0.19	0.03	0.22
160	20	1.34	1.33	4.02	1.34	1.19	3.57	0.15	0	0.15
160	20	1.78	1.78	5.35	1.78	1.64	4.93	0.14	0	0.14
160	20	2.23	2.23	6.69	2.23	2.07	6.2	0.17	0	0.17
160	20	2.68	2.67	8.03	2.68	2.54	7.63	0.13	0	0.13
180	20	2.23	2.23	6.69	2.23	2.05	6.17	0.17	0.01	0.18
220	20	1.78	1.78	5.35	1.78	1.53	4.77	0.17	0.09	0.25
220	20	2.23	2.23	6.69	2.23	1.98	6.13	0.16	0.1	0.25
220	20	2.68	2.67	8.03	2.68	2.41	7.44	0.16	0.1	0.27

[a]$F_{i,in}$ represents for the molar flow of the inlet stream component i, i = N_2, CO_2, and H_2

[b]$F_{i,out}$ represents for the molar flow of the outlet stream component i, i = N_2, CO_2, H_2, CH_3OH, CO, and H_2O

Table 4 The correlated kinetic parameters for the single-site kinetic model

Parameter	A_i	Unit	B_i	Unit
K_a	4.20 ± 0.91	bar$^{-0.5}$	− 5.37 ± 0.26	kJ·mol^{-1}
K_b	24.53 ± 1.18	bar^{-1}	− 9.38 ± 2.21	kJ·mol^{-1}
K_c	493.40 ± 11.18	/	− 2.05E-04 ± 1.38E-04	kJ·mol^{-1}
k_1	189.89 ± 9.06	mmol·g^{-1}·min^{-1}·bar^{-1}	34.24 ± 3.52	kJ·mol^{-1}
k_2	0.31 ± 0.14	mmol·g^{-1}·min^{-1}·bar^{-2}	121.60 ± 5.60	kJ·mol^{-1}

Table 5 The correlated kinetic parameters for the dual-site kinetic model

Parameter	A_i	Unit	B_i	Unit
k_1	20.49 ± 0.13	mmol·g^{-1}·min^{-1}·bar$^{-2.5}$	40.17 ± 0.18	kJ·mol^{-1}
k_2	10.30 ± 0.62	mmol·g^{-1}·min^{-1}·bar^{-2}	135.66 ± 1.22	kJ·mol^{-1}
K_{a1}	0.7207 ± 0.0068	bar^{-1}	− 5.88 ± 0.10	kJ·mol^{-1}
K_{a2}	641.00 ± 40.01	bar^{-1}	− 33.71 ± 0.18	kJ·mol^{-1}
K_{a3}	1.08 ± 0.0074	bar^{-1}	− 9.20 ± 0.65	kJ·mol^{-1}
K_{b1}	9.10 ± 0.11	bar$^{-0.5}$	− 13.68 ± 0.47	kJ·mol^{-1}
K_{b2}	452.56 ± 15.14	bar^{-1}	− 14.94 ± 0.86	kJ·mol^{-1}

12,000 ml·g^{-1}·h^{-1}. It can be seen that, from Fig. 7, changes in H2/CO2 ratio have a significant effect on CO_2 conversion. When the concentration of hydrogen in the feed gas is increased, the CO_2 conversion remarkably rises. Meanwhile, the selectivity of methanol increases simultaneously, which again agreed with the above thermodynamic simulations.

3.3 Identification of Kinetic Models

3.3.1 The Kinetic Measurements

Based on the results of above catalytic tests on activity and selectivity, the reaction conditions were adjusted and given in Table 3, using a mixture of CO_2/H_2/N_2 with varied

Table 6 Model statistical checklist for the single-site kinetic model

Component	Experimental data points (N)	Model degree of freedom (M)	Decisive index[a] (ρ^2)	F[b]	$F_{0.05}$ (M,N-M-1)
CO_2	18	10	0.99979	5895.40	3.65
H_2	18	10	0.99977	5436.98	3.65
CH_3OH	18	10	0.97951	59.76	3.65
H_2O	18	10	0.98306	72.54	3.65
CO	18	10	0.99743	485.07	3.65

[a] $\rho^2 = 1 - \sum_{i=1}^{N} \left(y_{i,e} - y_{i,c}\right)^2 / \sum_{i=1}^{N} \left(y_{i,e}\right)^2$.
[b] $F = [\sum_{i=1}^{N} \left(y_{i,e}\right)^2 - \sum_{i=1}^{N} \left(y_{i,e} - y_{i,c}\right)^2]/M / \sum_{i=1}^{N} \left(y_{i,e} - y_{i,c}\right)^2/N - M$.

Table 7 Model statistical checklist for the dual-site kinetic model

Component	Experimental data points (N)	Model degree of freedom (M)	Decisive index (ρ^2)	F	$F_{0.05}$ (M,N-M-1)
CO_2	18	12	0.99973	7483.75	4.68
H_2	18	12	0.99976	8241.55	4.68
CH_3OH	18	12	0.97228	70.14	4.68
H_2O	18	12	0.98779	161.74	4.68
CO	18	12	0.97865	91.68	4.68

compositions as feed gas for the kinetic measurements. CO_2 conversion and product selectivity were investigated with the variation of reaction temperatures and WHSV, respectively.

3.3.2 The Correlations for Kinetic Parameters

In this work, we assume that the data in Table 3 was obtained in a perfect differential reactor, in which the pressure drop was negligible (as compared to the operation pressure 2.0 Mpa, the pressure drop of the catalyst bed is 8.7 kPa calculated by the Ergun equation). Besides, the reactor was also considered as under an isothermal condition. Then the mathematical model of reaction rate, Eq. (15), can be then solved by using the Rung-Kutta methods [30], ode45 in Matlab, with the initial boundary of the entire reactor obtained using the inlet gas composition, Eq. (16).

$$R_i = \frac{dF_i}{d\left(W_{cat}\right)} = \sum_m v_{m,i} r_m \tag{17}$$

$$F_i = F_{i0} \text{ at } W_{cat} = 0 \tag{18}$$

Besides, the kinetic parameters were estimated according to the minimization of the square differences between experimental and calculated results, as shown by Eq. (17), using Isqnonlin optimization algorithm in Matlab software.

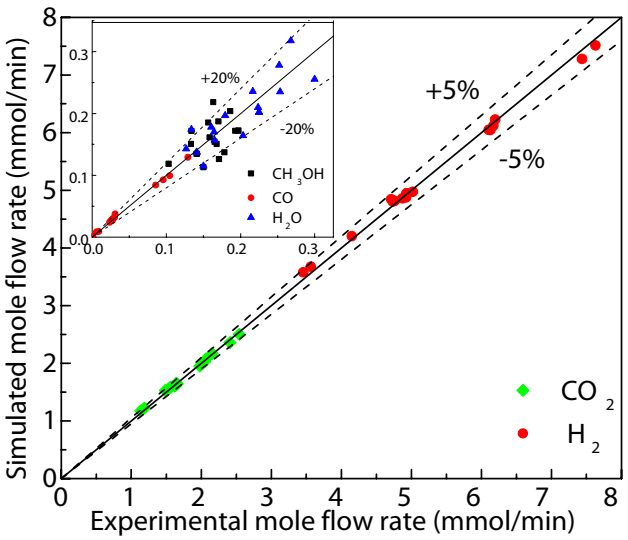

Fig. 8 Parity plot of outlet molar flow rates for single-site model

$$s = (\sum_j \left[(F_{co,e,j} - F_{co,c,j})^2\right) + (F_{MeOH,e,j} - F_{MeOH,c,j})^2] \tag{19}$$

where $F_{co,e,j}$ represents the molar flow of CO in experimental running j, and $y_{co,c,j}$ the calculated value by the mathematical model under the corresponding conditions of running j; Similarly, $F_{MeOH,e,j}$ represents the molar flow of CH_3OH in experimental running j, and $F_{MeOH,c,j}$ the calculated value of the molar flow of CH_3OH.

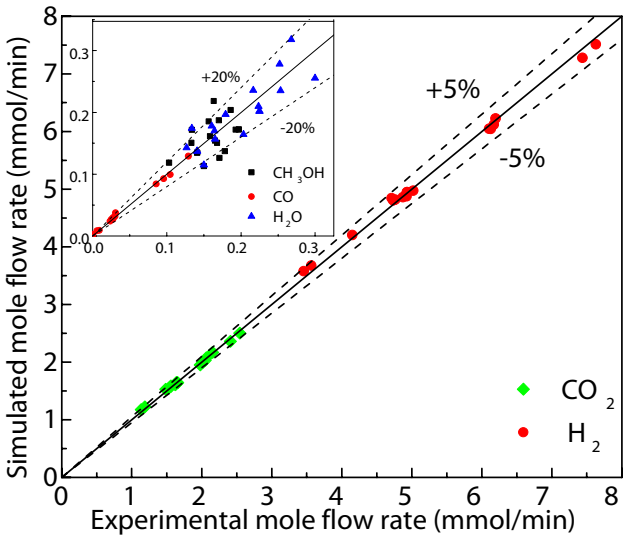

Fig. 9 Parity plot of outlet molar flow rates for dual-site mechanism

Considering the experimental results obtained in Table 3, the values of model parameters can be estimated for both single-site kinetic model (Table 4) and dual-site kinetic model (Table 5).

It can be seen that the activation energy for methanol synthesis and RWGS reaction are 34.24 kJ·mol^{-1} and 121.60 kJ·mol^{-1} for single-site kinetic model, and 40.17 kJ·mol^{-1} and 135.66 kJ·mol^{-1} for dual-site kinetic model, respectively. These values are well consistent with the previous published reports, in which the given activation energy ranges 30–70 kJ·mol^{-1} for methanol synthesis and 95–155 kJ·mol^{-1} for RWGS reaction [36, 41–45]. On the other hand, the adsorption heats for both models were calculated and are given as negative, again meaning that our modifications are feasible in terms of these two models. Particularly, in the single-site model, the adsorption heats are very low, with that of oxygen nearly zero, which is agreed well with Vanden Bussche and Froment [25]. The H adsorption heats in the present work (for both single-site and dual-site model) are similar with the previous report [25]. While the H_2O adsorption heats are relatively low as compared with Vanden Bussche and Fromment [25], as H_2O is strongly adsorbed over the catalyst within the operation temperatures (see Fig. 11b), leading to its adsorption variation limited with the increasing of operation temperatures.

3.3.3 Comparison of the Kinetic Models

At this point, the experimental results of catalytic tests were successfully modeled using the kinetic and adsorption coefficients based the single-site and dual-site Langmuir–Hinshelwood mechanisms. In this section, a comparison between these two models is demonstrated. First of all, the single-site model includes the adsorption of H_2, H_2O, and O with neglecting carbon monoxide and carbon dioxide. By contrast, the dual-site model includes H_2 and H_2O on one site, as well as CO and CO_2 on the other site, as shown by Eq. (7), Eq. (8), and Eq. (12), Eq. (13), which seems to be more reasonable. From Table 5, one can notice that, the adsorption of both CO and H_2O are dominant on the two sites, respectively, and increasing temperature will weaken the adsorption of the CO and H_2O due to the exothermicity of the adsorption.

Secondly, Table 6 and Table 7 present the statistical checklists of the model estimations for the single-site and dual site models, respectively. As Vanden Bussche and Froment demonstrated, due to the nonlinear characteristic of the model, the F test is very indicative. From Table 6 and Table 7, the obtained F values are both much larger than the tabulated 95% value. Thus, it can be seen that in the present study, the model statistical checklists in Tables 6 and 7 reveal that both optimized models have satisfactory correlation performance for CO_2 hydrogenation to methanol over the tested Cu/ZnO/Al_2O_3.

Furthermore, the parity plots for both kinetic models are shown in Figs. 8, 9, based on the molar rate for each reactant/product in the outlet stream. It can be seen that both models with the optimized parameters are able to describe well the experimental points within a relative deviation smaller than 20%, and less than 5% for CO_2 and H_2 in particular.

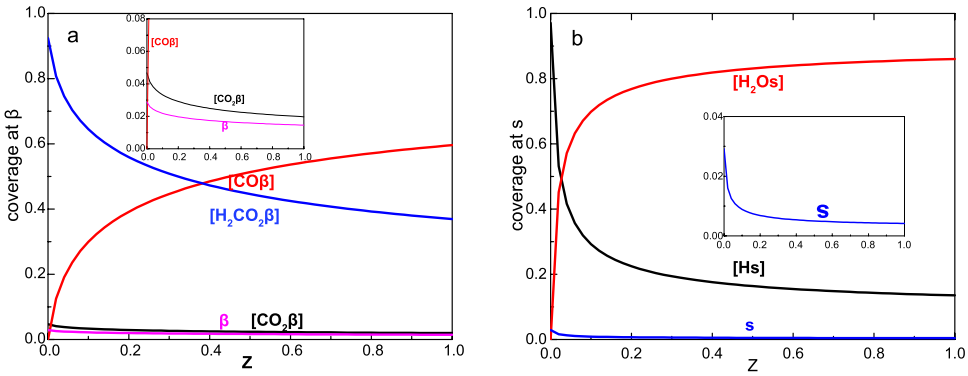

Fig. 10 Evolution of the adsorbate coverages in the reactor (200^{O}C, 30 bar, H_2: CO_2 = 5:1). **a**: β-site, **b**: s-site

Nevertheless, as for the average sum of errors of CO and CH_3OH, the single-site model endowed a value of 0.0263, while the dual-site model 0.0139. In this sense, it can be deduced modestly that the dual-site model fits the experimental results better than the single-site model.

3.4 Discrimination of the Key Adsorbed Species

As compared to the single-site model, the dual-site model's advantage is that it involves more key species adsorbed on the catalyst surface, not only the reactants CO_2 and H_2 but also the products CO and H_2O, and especially an intermediate, the formate, H_2CO_2 as well, which is generally considered as a pivotal intermediate for methanol generation on the Cu/ZnO/Al_2O_3 catalyst when the feedstock consists of CO_2. The results reveal that the formed CO and H_2O during the reaction will have remarkable inhibitive impact on the production of CH_3OH, and can be illustrated by the dual-site model very well. Therefore, it is believable that the dual-site model is more reasonable and is a solid guidance for methanol production from CO_2 hydrogenation over the conventional Cu/ZnO/Al_2O_3 catalyst from the viewpoint of industrialization.

Accordingly, the impacts of reaction conditions on the adsorbed key species (CO_2, CO, H, H_2O, and H_2CO_2) are worth of discussion. From the theory of Langmiur –Hinshelwood adsorption and reaction on catalyst surface, Formula (18–24) are derived for estimation of the adsorbed species involved.

$$[CO_2\beta] = \frac{K_{a1}P_{CO_2}}{1 + K_{a1}P_{CO_2} + K_{a2}P_{CO} + K_{a3}P_{CO_2}P_{H_2}} \tag{20}$$

$$[\mathrm{CO}\beta] = \frac{K_{a2}P_{CO}}{1 + K_{a1}P_{CO_2} + K_{a2}P_{CO} + K_{a3}P_{CO_2}P_{H_2}} \tag{21}$$

$$[\mathrm{H_2CO_2}\beta] = \frac{K_{a3}P_{CO_2}P_{H_2}}{1 + K_{a1}P_{CO_2} + K_{a2}P_{CO} + K_{a3}P_{CO_2}P_{H_2}} \tag{22}$$

$$[\beta] = \frac{1}{1 + K_{a1}P_{CO_2} + K_{a2}P_{CO} + K_{a3}P_{CO_2}P_{H_2}} \tag{23}$$

$$[\mathrm{Hs}] = \frac{K_{b1}P_{H_2}^{0.5}}{1 + K_{b1}P_{H_2}^{0.5} + K_{b2}P_{H_2O}} \tag{24}$$

$$[H_2Os] = \frac{K_{b2}P_{H_2O}}{1 + K_{b1}P_{H_2}^{0.5} + K_{b2}P_{H_2O}} \tag{25}$$

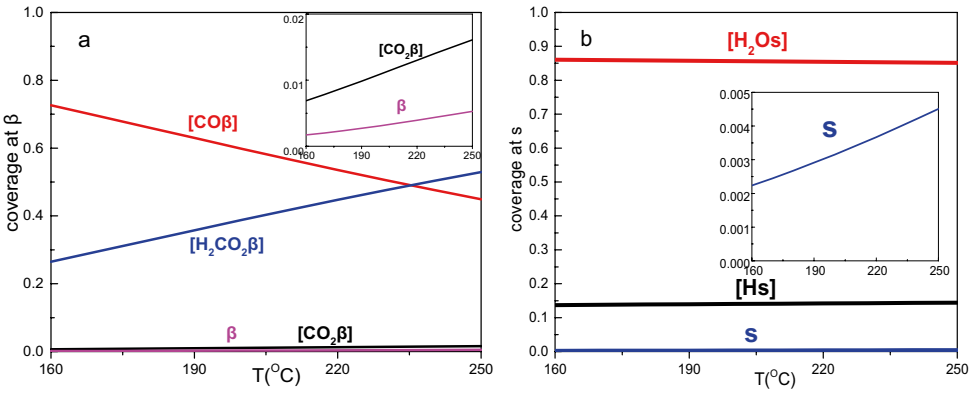

Fig. 11 Temperature effect on adsorbate coverages at the reactor exit (30 bar, H_2: CO_2 = 5:1). The solid curves present the coverages of intermediates on β-site, and the dashed on s-site

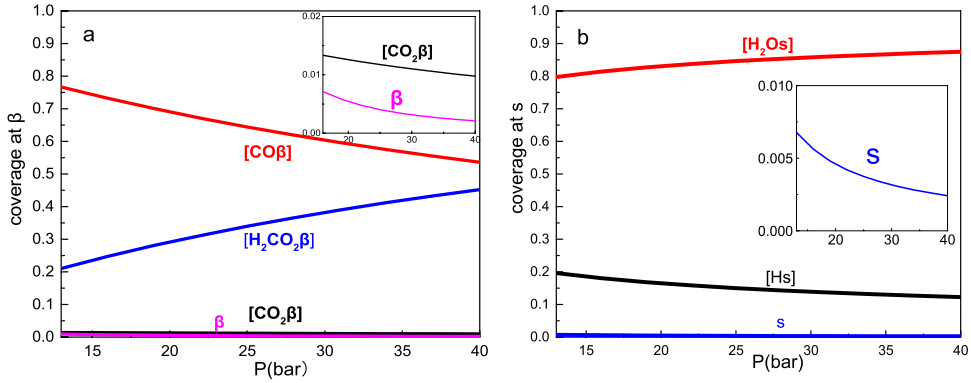

Fig. 12 Pressure effect on adsorbate coverages at the reactor exit (200°C, H_2:CO_2 = 5:1). **a**: β-site, **b**: s-site

$$[s] = \frac{1}{1 + K_{b1}P_{H_2}^{0.5} + K_{b2}P_{H_2O}} \quad (26)$$

Figure 10 reveals the evolution of the adsorbate coverages on the active sites in the laboratory reactor at the operating conditions: 200 °C, 30 bar, H_2: CO_2 = 5:1. It can be noticed that, at the entrance of the reactor, both formate and atomic hydrogen are absolutely predominant adsorbed on the two active sites, respectively, with the vacancy percentage nearly zero at the studied conditions. As far as the s site, which is for [Hs] and [H_2Os], [Hs] is replaced by [H_2Os] in no time after the reaction is ignited near the inlet, and [H_2Os] is responsible for 80% of the active sites when the reactant mixture flows through the position at 30% percentage of the total reactor length, which means the product H_2O has strong inhibition to hydrogen adsorption, and thus to the methanol synthesis reaction. On the other hand, on active site β, which is assumed for the carbonous species, the formate species (formic acid), [$HCO_2H\beta$], generated by the first hydrogenation of the adsorbed CO_2, [$CO_2\beta$], with the adsorbed atomic hydrogen, [Hs], takes most of the active positions initially °Ccupied by CO_2, i.e., [$HCO_2H\beta$] = 0.92, [$CO_2\beta$] = 0.045, and the vacancy [β] = 0.035, and it is gradually substituted by the CO adsorption with a fractional coverage of CO, [COβ] surpassing that of formate at the reactor length about 0.35, which implies that in the later period of the reaction, CO desorption may become the rate-determining step (RDS) for the reverse water gas shift reaction (RWGS).

Figure 11 displays the influence of temperature on the adsorbate coverages. It can be seen that, on the active site for H_2 and H_2O, s, [H_2Os] predominates over [Hs], and always is over 80%, which means the H_2O is strongly sticked on the active site s and inhibits the H_2 adsorption. Unexpectedly, the temperature has a little impact on this behavior. On the other hand, on the other site, β, for CO, CO_2 and formate, the impact of temperature is significant on CO and CO_2 adsorbates. With the rise of temperature, the concentration of [formate-β] increases obviously and that of [COβ] decreases correspondingly. Strangely, [$CO_2\beta$] changes little with change of temperature. Therefore, higher temperature favors the formate adsorption, leading to the reactions turn into the right-hand site, achieving higher CO_2 conversion. Furthermore, at the reactor outlet, the vacancy percentages for both s and β sites, are very closed to zero, less than 0.5%, implying excessively strong inhibition by the adsorbates.

The influence of pressure on the adsorbate coverages is showed in Fig. 12. One can see that the pressure has little influence on [CO_2] adsorption, but has obvious influence on the other adsorption species. The adsorption concentrations of [H_2O] and [H_2CO_2] increase with the increase of pressure, while the adsorption concentrations of [CO] and [H] decrease with the increase of pressure. Therefore, the increase of pressure is beneficial to increase the selectivity of methanol and reduce the selectivity of CO. However, when the pressure is greater than 2.0Mpa, the change of adsorption concentration of [CO] and [H_2CO_2] slows down, which also proves that the studied Cu/ZnO/Al_2O_3 catalyst is a low-pressure CO_2 hydrogenation catalyst to methanol.

In a word, from the analysis showed above, one can be convinced that methanol synthesis from CO_2 hydrogenation suffers an extremely strong adsorption inhibition from the by-products water and carbon monoxide, and besides that, a stronger inhibition comes from the intermediate formate.

4 Conclusions

In this work, the hydrogenation of CO_2 to methanol has been tested on a commercial Cu/ZnO/Al_2O_3 catalyst. Effects of operating conditions on the catalytic activity were investigated by a thermodynamic study and contrasted experimentally. The catalyst was tested in a lab integral reactor using a feed mixture of $CO_2/H_2/N_2$ with varied compositions under 160–250 °C, 1.0–2.5 MPa, and H_2/CO_2 ratio of 2–10. The results demonstrated that the methanol synthesis from CO_2 is favored by lower temperatures, higher pressures, and higher H_2/CO_2 ratio.

Besides, we have identified the kinetic models and parameters for the methanol synthesis from CO_2 under the studies conditions based on two mechanisms of single-site and dual-site absorption, the corresponding models both match the experimental data fairly well, meaning both the single-site and dual-site mechanisms are reasonable for CO_2 hydrogenation to methanol on the Cu-based catalyst. Nevertheless, by comparison with the single-site model, the dual-site model fit the experimental results more accurately since its average sum of error is smaller, and more reasonable as the result of including both CO and CO_2 adsorption, and of speculating the strong inhibition both of CO and H_2O. Finally, we further verified the rationality of the experimental results and the dynamics of the dual-site model by calculating and analyzing the coverages of intermediates, which shows the formate intermediate is surely the predominant adsorbate though H_2O and CO have equivalently strong adsorption with the respective active sites with nearly little vacant sites reserved.

Overall, the present work offers a comprehensive study from simulation to experimental tests for CO_2 hydrogenation to methanol over Cu/ZnO/Al_2O_3 catalyst, which may pave the way towards optimisation of catalysts design and process conditions for direct CO_2 to methanol conversion, a key reaction within the circular economy concept.

Acknowledgements The authors would like to thank the 2019 Key Technology Project of Inner Mongolia (No. 2019GG311, China), and Royal Society Research Grant (No. RSRG1180353, UK) for supporting this work.

References

1. Lindsey R, Dlugokencky E (Oct 2021) https://www.climate.gov/news-features/understanding-climate/climate-change-atmospheric-carbon-dioxide. Climate Change: Atmospheric Carbon Dioxide.
2. Li B, Gasser T, Ciais P, Piao S, Tao S, Balkanski Y, Hauglustaine D, Boisier JP, Chen Z, Huang MT, Li LZX, Li Y, Liu H, Liu J, Peng S, Shen Z, Sun Z, Wang R, Wang T, Yin G, Yin Y, Zeng H, Zeng Z, Zhou F (2016) The contribution of China's emissions to global climate forcing. Nature 531:357–361. https://doi.org/10.1038/nature17165
3. Anderson TR, Hawkins E, Jones PD (2016) CO_2, the greenhouse effect and global warming: from the pioneering work of Arrhenius and Callendar to today's Earth System Models. Endeavour 40:178–187. https://doi.org/10.1016/j.endeavour.2016.07.002
4. Szulejko JE, Kumar P, Deep A, Kim KH (2017) Global warming projections to 2100 using simple CO_2 greenhouse gas modeling and comments on CO_2 climate sensitivity factor. Atmos Pollu Res 8:136–140. https://doi.org/10.1016/j.apr.2016.08.002
5. Hepburn C, Adlen R, Beddington J, Carter EA, Fuss S, Dowell NM, Minx JC, Smith P, Williams CK (2019) The technological and economic prospects for CO_2 utilization and removal. Nature 575:87–96. https://doi.org/10.1038/s41586-019-1681-6
6. Gao W, Liang S, Wang R, Jiang Q, Zhang Y, Zheng Q, Xie B, Toe CY, Zhu X, Wang J, Huang L, Gao Y, Wang Z, Jo C, Wang Q, Wang L, Liu Y, Louis B, Scott J, Roger JC, Amal R, He H, Park SE (2020) Industrial carbon dioxide capture and utilization: state of the art and future challenges. Chem Soc Rev 49:8584–8686. https://doi.org/10.1039/D0CS00025F
7. Kamkeng ADN, Wang M, Hu J, Du WL, Qian F (2021) Transformation technologies for CO_2 utilisation: Current status, challenges and future prospects. Chem Eng J 409:128138. https://doi.org/10.1016/j.cej.2020.128138
8. Jiang K, Ashworth P, Zhang S, Liang X, Sun Y (2020) China's carbon capture, utilization and storage (CCUS) policy: A critical review. Renew Sust Energ Rev 119:109601. https://doi.org/10.1016/j.rser.2019.109601
9. Olah GA (2005) Beyond oil and gas: The methanol economy. Angew Chem Int Edit 44:2636–2639. https://doi.org/10.1002/anie.200462121
10. Stephan DW (2013) A step closer to a methanol economy. Nature 495:54–55. https://doi.org/10.1038/nature11955
11. Dalena F, Senatore A, Marino A, Gordano A, Basile M, Basile A (2018) Methanol Science and Engineering. Elsevier, Amsterdam
12. Zhong JW, Yang XF, Wu ZL, Liang BL, Huang YQ, Zhang T (2020) State of the art and perspectives in heterogeneous catalysis of CO_2 hydrogenation to methanol. Chem Soc Rev 49:1385–1413. https://doi.org/10.1039/C9CS00614A
13. Sharma P, Sebastian J, Ghosh S, Creaser D, Olsson L (2021) Recent advances in hydrogenation of CO_2 into hydrocarbons via methanol intermediate over heterogeneous catalysts. Catal Sci Technol 11:1665–1697. https://doi.org/10.1039/D0CY01913E
14. Navarro-Jaén S, Virginie M, Bonin J, Robert M, Wojcieszak R, Khodakov AY (2021) Highlights and challenges in the selective reduction of carbon dioxide to methanol. Nat Rev Chem 5:566–581. https://doi.org/10.1038/s41570-021-00289-y
15. Rivera-Tinoco R, Farran M, Bouallou C, Aupretre F, Valentin S, Millet P, Ngameni JR (2016) Investigation of power-to-methanol processes coupling electrolytic hydrogen production and catalytic CO_2 reduction. Inter J Hydro Energy 41:4546–4549. https://doi.org/10.1016/j.ijhydene.2016.01.059
16. Bos MJ, Kersten SRA, Brilman DWF (2020) Wind power to methanol: Renewable methanol production using electricity, electrolysis of water and CO_2 air capture. Appl Energy 264:114672. https://doi.org/10.1016/j.apenergy.2020.114672
17. Lonis F, Tola V, Cau G (2021) Assessment of integrated energy systems for the production and use of renewable methanol by water electrolysis and CO_2 hydrogenation. Fuel 285:119160. https://doi.org/10.1016/j.fuel.2020.119160
18. Biernacki P, Rother T, Paul W, Werner P, Steinigeweg S (2018) Environmental impact of the excess electricity conversion into methanol. J Clean Prod 191:87–98. https://doi.org/10.1016/j.jclepro.2018.04.232
19. Kim H, Kim A, Byun M, Lim H (2021) Comparative feasibility studies of H_2 supply scenarios for methanol as a carbon-neutral H_2 carrier at various scales and distances. Renew Energy 180:552–559. https://doi.org/10.1016/j.renene.2021.08.077
20. Olah GA, Goeppert A, Surya Prakash GK (2009) Beyond Oil and Gas: The Methanol Economy. Wiley, Hoboken
21. Studt F, Abild-Pedersen F, Wu Q, Jensen AD, Temel B, Grunwaldt JF, Norskov JK (2012) CO hydrogenation to methanol on Cu–Ni catalysts: Theory and experiment. J Catal 293:51–60. https://doi.org/10.1016/j.jcat.2012.06.004
22. Pokrovski KA, Bell AT (2006) An investigation of the factors influencing the activity of Cu/CexZr1− xO_2 for methanol synthesis via CO hydrogenation. J Catal 241:276–286. https://doi.org/10.1016/j.jcat.2006.05.002
23. Pokrovski KA, Bell AT (2006) Effect of dopants on the activity of Cu/$M_{0.3}Zr_{0.7}O_2$ (M= Ce, Mn, and Pr) for CO hydrogenation to methanol. J Catal 244:43–51. https://doi.org/10.1016/j.jcat.2006.07.031
24. Graaf GH, Stamhuis EJ, Beenackers AACM (1988) Kinetics of low-pressure methanol synthesis. Chem Eng Sci 43:3185–3195. https://doi.org/10.1016/0009-2509(88)85127-3
25. Bussche KV, Froment G (1996) A steady-state kinetic model for methanol synthesis and the water gas shift reaction on a commercial Cu/ZnO/Al_2O_3Catalyst. J Catal 161:1–10. https://doi.org/10.1006/jcat.1996.0156
26. Ovesen CV, Clausen BS, Schiøtz J, Stoltze P, Topsøe H, Nørskov JK (1997) Kinetic implications of dynamical changes in catalyst morphology during methanol synthesis over Cu/ZnO catalysts. J Catal 168:133–142. https://doi.org/10.1006/jcat.1997.1629
27. Park N, Park MJ, Lee YJ, Ha KS, Jun KW (2014) Kinetic modeling of methanol synthesis over commercial catalysts based on three-site adsorption. Fuel Process Technol 125:139–147. https://doi.org/10.1016/j.fuproc.2014.03.041
28. Seidel C, Jörke A, Vollbrecht B, Seidel-Morgenstern A, Kienle A (2018) Kinetic modeling of methanol synthesis from renewable resources. Chem Eng Sci 175:130–138. https://doi.org/10.1016/j.ces.2017.09.043
29. Ledakowicz S, Nowicki L, Petera J, Niziol J, Kowalik P, Golebiowski A (2013) Kinetic characterisation of catalysts for methanol synthesis. Chem Process Enginz 34:497–506. https://doi.org/10.2478/cpe-2013-0040
30. Kobl K, Thomas S, Zimmermann Y, Parkhomenko K, Roger A (2016) Power-law kinetics of methanol synthesis from carbon dioxide and hydrogen on copper–zinc oxide catalysts with alumina or zirconia supports. Catal Today 270:31–42. https://doi.org/10.1016/j.cattod.2015.11.020
31. Rasmussen PB, Holmblad PM, Askgaard T, Ovesen CV, Stoltze P, Norskov JK, Chorkendorff I (1994) Methanol synthesis on

Cu (100) from a binary gas mixture of CO_2 and H_2. Catal Lett 26:373–381. https://doi.org/10.1007/BF00810611
32. Portha JF, Parkhomenko K, Kobl K, Roger AC, Arab S, Commenge JM, Falk L (2017) Kinetics of methanol synthesis from carbon dioxide hydrogenation over copper–zinc oxide catalysts. Ind Eng Chem Res 56:13133–13145. https://doi.org/10.1021/acs.iecr.7b01323
33. Chinchen GC, Waugh KC, Whan DA (1986) The activity and state of the copper surface in methanol synthesis catalysts. Appl Catal 25:101–107. https://doi.org/10.1016/S0166-9834(00)81226-9
34. Clarke DB, Bell AT (1995) An infrared study of methanol synthesis from CO_2 on clean and potassium-promoted Cu/SiO_2. J Catal 154:314–328. https://doi.org/10.1006/jcat.1995.1173
35. Graaf GH, Sijtsema P, Stamhuis EJ, Joosten GEH (1986) Chemical equilibria in methanol synthesis. Chem Eng Sci 41:2883–2890. https://doi.org/10.1016/0009-2509(86)80019-7
36. Yoshihara J, Parker SC, Schafer A, Campbell CT (1995) Methanol synthesis and reverse water-gas shift kinetics over clean polycrystalline copper. Catal Lett 31:313–324. https://doi.org/10.1007/BF00808595
37. Ayastuy JL, Gutie´rrez-Ortiz MA, Gonza´lez-Marcos JA, Aranzabal A, Gonza´lez-Velasco JR (2005) Kinetics of the Low-Temperature WGS Reaction over a CuO/ZnO/Al_2O_3 Catalyst. Ind Eng Chem Res 44:1–50. https://doi.org/10.1021/ie049886w
38. Mendes D, Chibante V, Mendes A, Madeira LM (2010) Determination of the low-temperature water-gas shift reaction kinetics using a Cu-based catalyst. Ind Eng Chem Res 49(2010):11269–11279. https://doi.org/10.1021/ie101137b
39. Madon RJ, Braden D, Kandoi S, Nagel P, Mavrikakis M, Dumesic JA (2011) Microkinetic analysis and mechanism of the water gas shift reaction over copper catalysts. J Catal 281:1–11. https://doi.org/10.1016/j.jcat.2011.03.008
40. Kunkes EL, Studt F, Abild-Pedersen F, Schlögl R, Behrens M (2015) Hydrogenation of CO_2 to methanol and CO on Cu/ZnO/Al_2O_3: Is there a common intermediate or not? J Catal 328:43–48. https://doi.org/10.1016/j.jcat.2014.12.016
41. Chinchen GC, Denny PJ, Parker DG, Spencer MS, Whan DA (1987) Mechanism of methanol synthesis from CO_2/CO/H_2 mixtures over copper/zinc oxide/alumina catalysts: use of 14C-labelled reactants. Appl Catal 30:333–338. https://doi.org/10.1016/s0166-9834(00)84123-8
42. Karelovic A, Ruiz P (2015) The role of copper particle size in low pressure methanol synthesis via CO_2 hydrogenation over Cu/ZnO catalysts. Catal Sci Technol 5:869–881. https://doi.org/10.1039/C4CY00848K
43. Słoczyński J, Grabowski R, Olszewski P, Kozlowska A, Stoch J, Lachowska M, Skrzypek J (2006) Effect of metal oxide additives on the activity and stability of Cu/ZnO/ZrO_2 catalysts in the synthesis of methanol from CO_2 and H_2. Appl Catal A 310:127–137. https://doi.org/10.1016/j.apcata.2006.05.035
44. Chou CY, Lobo RF (2019) Direct conversion of CO_2 into methanol over promoted indium oxide-based catalysts. Appl Catal A 583:117144. https://doi.org/10.1016/j.apcata.2019.117144
45. Choi Y, Futagami K, Fujitani T, Nakamura J (2001) The role of ZnO in Cu/ZnO methanol synthesis catalysts—morphology effect or active site model. Appl Catal A 208:163–167. https://doi.org/10.1016/S0926-860X(00)00712-2